

**Nerve detection using optical spectroscopy, an evaluation in four different models
In human and swine, in-vivo, and post mortem**

Langhout, Gerrit C.; Bydlon, Torre M.; van der Voort, Marjolein; Müller, Manfred; Kortsmits, Jeroen; Lucassen, Gerald; Balthasar, Andrea J.R.; van Geffen, Geert Jan; Steinfeldt, Thorsten; Sterenborg, Henricus J.C.M.

DOI

[10.1002/lsm.22755](https://doi.org/10.1002/lsm.22755)

Publication date

2018

Document Version

Final published version

Published in

Lasers in Surgery and Medicine

Citation (APA)

Langhout, G. C., Bydlon, T. M., van der Voort, M., Müller, M., Kortsmits, J., Lucassen, G., Balthasar, A. J. R., van Geffen, G. J., Steinfeldt, T., Sterenborg, H. J. C. M., Hendriks, B. H. W., & Ruers, T. J. M. (2018). Nerve detection using optical spectroscopy, an evaluation in four different models: In human and swine, in-vivo, and post mortem. *Lasers in Surgery and Medicine*, 50(3), 253-261. <https://doi.org/10.1002/lsm.22755>

Important note

To cite this publication, please use the final published version (if applicable).
Please check the document version above.

Copyright

Other than for strictly personal use, it is not permitted to download, forward or distribute the text or part of it, without the consent of the author(s) and/or copyright holder(s), unless the work is under an open content license such as Creative Commons.

Takedown policy

Please contact us and provide details if you believe this document breaches copyrights.
We will remove access to the work immediately and investigate your claim.

Nerve Detection Using Optical Spectroscopy, an Evaluation in Four Different Models: In Human and Swine, In-Vivo, and Post Mortem

Gerrit C. Langhout, MD,^{1*} Torre M. Bydlon, PhD,² Marjolein van der Voort, PhD,³ Manfred Müller, PhD,² Jeroen Kortzmit, PhD,³ Gerald Lucassen, PhD,³ Andrea J.R. Balthasar, MD,⁴ Geert-Jan van Geffen, MD, PhD,⁵ Thorsten Steinfeldt, MD, PhD,⁶ Henricus J.C.M. Sterenborg, PhD,⁷ Benno H.W. Hendriks, PhD,^{2,8} and Theo J.M. Ruers, MD, PhD^{1,9}

¹Department of Surgery, The Netherlands Cancer Institute—Antoni van Leeuwenhoek, Plesmanlaan 121, 1066 CX Amsterdam, The Netherlands

²Philips Research, In-Body Systems Department, HTC 34, 5656 AE Eindhoven, The Netherlands

³Philips HealthTech, Veenpluis 4, 5684 PC, Best, The Netherlands

⁴Department of Anesthesiology and Pain Medicine, Maastricht University Medical Center, P. Debyelaan 25, 6229 HX, Maastricht, The Netherlands

⁵Department of Anesthesiology, Radboud Medical Center, Radboud University, Geert Grooteplein Zuid 10, 6525 GA, Nijmegen, The Netherlands

⁶Diakonie-Klinikum Schwäbisch Hall, Department of Anesthesia, Diakoniestraße 10, 74523 Schwäbisch Hall, Germany

⁷Department of Biomedical Engineering and Physics, Amsterdam Medical Center, Meibergdreef 9, 1105 AZ Amsterdam, the Netherlands

⁸Department of BioMechanical Engineering, Delft University of Technology, Mekelweg 2, 2628 CD, Delft, The Netherlands

⁹Nanobiophysics Group, MIRA Institute, University of Twente, Post Box 217, 7500 AE Enschede, The Netherlands

Objective: Identification of peripheral nerve tissue is crucial in both surgery and regional anesthesia. Recently, optical tissue identification methods are presented to facilitate nerve identification in transcutaneous procedures and surgery. Optimization and validation of such techniques require large datasets. The use of alternative models to human *in vivo*, like human post mortem, or swine may be suitable to test, optimize and validate new optical techniques. However, differences in tissue characteristics and thus optical properties, like oxygen saturation and tissue perfusion are to be expected. This requires a structured comparison between the models.

Study Design: Comparative observational study.

Methods: Nerve and surrounding tissues in human (*in vivo* and post mortem) and swine (*in vivo* and post mortem) were structurally compared macroscopically, histologically, and spectroscopically. Diffuse reflective spectra were acquired (400–1,600 nm) after illumination with a broad band halogen light. An analytical model was used to quantify optical parameters including concentrations of optical absorbers.

Results: Several differences were found histologically and in the optical parameters. Histologically nerve and adipose tissue (subcutaneous fat and sliding fat) showed clear similarities between human and swine while human muscle enclosed more adipocytes and endomysial collagen. Optical parameters revealed model dependent differences in concentrations of β -carotene, water, fat, and oxygen saturation. The similarity between optical parameters is, however, sufficient to yield a strong positive correlation after cross model classification.

Conclusion: This study shows and discusses similarities and differences in nerve and surrounding tissues between human *in vivo* and post mortem, and swine *in vivo* and post mortem; this could support the discussion to use an alternative model to optimize and validate optical techniques for clinical nerve identification. *Lasers Surg. Med.* 50:253–261, 2018. © 2017 Wiley Periodicals, Inc.

Key words: optical spectroscopy; diffuse reflectance spectroscopy; nerve identification; human and animal authors have any conflicts of interest.

Conflict of Interest Disclosures: All authors have completed and submitted the ICMJE Form for Disclosure of Potential Conflicts of Interest and have disclosed the following: The authors who are affiliated with Philips (T.B., MvdV, M.M., J.K., G.L., B.H.) are employees of Philips. The prototype system described in this article is a research prototype. None of the other authors have any conflicts of interest.

Contract grant sponsor: Philips Research, Eindhoven, the Netherlands; Contract grant sponsor: KWF-Alpe d'HuZes, Amsterdam, the Netherlands; Contract grant number: NKI 2014-6596.

*Correspondence to: Gerrit C. Langhout, MD, Department of Surgery, The Netherlands Cancer Institute—Antoni van Leeuwenhoek, Plesmanlaan 121, 1066 CX Amsterdam, The Netherlands. E-mail: n.langhout@nki.nl

Accepted 14 October 2017

Published online 21 November 2017 in Wiley Online Library (wileyonlinelibrary.com).

DOI 10.1002/lsm.22755

INTRODUCTION

Identification of peripheral nerves is crucial in both surgery and regional anesthesia. During surgery, nerves have to be identified and spared to prevent morbidity including pain, numbness, weakness, and paralysis. For regional anesthesia, real time feedback of the tissue type at the tip of a needle may improve accurate deposition of the analgesic and therefore improve the quality and onset of a nerve block.

Nerve identification techniques currently being used, like nerve elicitation of motor response or paresthesia, have low sensitivities (30–70% for electrical stimulation and 40% for mechanical stimulation [1,2] which indicate the clear need for more reliable techniques. Diffuse reflectance spectroscopy (DRS) is an optical technique which can characterize tissue based on differences in the optical absorption and scattering properties. In DRS, tissue is illuminated with a broad spectral light and the diffusely reflected light is measured. Each biological tissue has its intrinsic absorption and scattering properties which directly influence the reflected light that will be measured. Based on the measured spectrum, optical absorbers like hemoglobin, water, lipids, and β -carotene can be quantified. Both the quantified absorbers and the scattering parameters are used for further tissue identification. A number of studies show the potential of nerve identification using diffuse reflectance spectroscopy [3–8]. Two *in vivo* human studies are published but both were performed with a small number of measurements [6,8]. Optimization of the technique for *in vivo* human clearly demands validation on a large study population. Tissue classification algorithms utilized with optical spectroscopy data often rely on principal component analysis [9], classification and regression trees [10,11], or K-nearest neighbor principle [5]. A large number of measurements in the training sets of these algorithms will yield more reliable classification results. However, *in vivo* human validation of nerve detecting techniques has limitations. Especially the acquisition of extensive measurements in patients requires much preparation, attention, and care. Other models may be more appropriate, allowing more numerous, extensive and repeated measurements, contributing to a robust construction and validation of identification models. Examples of such models are human *post mortem* (i.e., cadaver) or in animal.

This study aims to expose and understand the similarities and differences to validate nerve measurements between human *in vivo*, human post mortem, swine *in vivo*, and swine *post mortem*. This could be of value when choosing a model to validate optical techniques for nerve identification. To this end spectroscopic data, histological slides, and anatomy were compared between the four models.

MATERIALS AND METHODS

Diffuse reflectance spectra were acquired from the nerves and surrounding tissues in four different models: human *in vivo*, human post mortem, swine *in vivo*, and

swine *post mortem*. Nerves included the femoral and sciatic nerve. All nerve measurements were performed by placing the instrument on the nerve, the nerve was never punctured. Surrounding tissue was categorized as subcutaneous fat, muscle and sliding fat. Sliding fat is defined as the fat surrounding the entire nerve bundle [5]. During measurements, the tissue of interest was covered and the surgical lights were dimmed to minimize the influence of environmental light.

Human In Vivo Measurements

Human *in vivo* measurements were performed at The Netherlands Cancer Institute—Antoni van Leeuwenhoek under approval of the protocol and ethics review board (NL40893.031.12). Patients undergoing inguinal lymph node dissection or resection of a soft tissue tumor located in the groin were included. Patients were selected based on the likelihood of exposure of the femoral or sciatic nerve. Eighteen patients were included, the diameter of the femoral or sciatic nerve at the measurement location varied from 1 to 13 mm. Comprehensive tissue classification and extensive description of the measured spectra of this human *in vivo* series are described earlier [12].

Human Post Mortem Measurements

Human *post mortem* measurements included measurements in four freshly frozen whole body specimens. Fresh frozen bodies are cooled down to -30°C without further preservation. After acclimatization to room temperature, the femoral nerve at both legs was exposed from the inguinal ligament over a trajectory of at least 10 cm. Branches of the femoral nerve were measured to a size of at least 2 mm diameter. The body was then rotated to allow exposure of the sciatic nerve. The sciatic nerve was exposed from 2 to 3 cm caudal from the ischial tuberosity toward the knee.

Swine In Vivo Measurements

Swine *in vivo* measurements were conducted under approval of the animal ethics committee (Utrecht University, Utrecht, the Netherlands). During the measurements, animals were anesthetized using isoflurane. The sciatic nerve was exposed over a trajectory of at least 10 cm. A total of six sciatic nerves were measured on three domestic pigs, diameter 4 to 8 mm.

Swine Post Mortem Measurements

Swine *post mortem* measurements were performed on six sciatic nerves, from three animals. Similar to the *in vivo* swine measurements, the nerve was exposed over a trajectory of at least 10 cm, the diameter of the measured nerves was 4 to 8 mm.

Anatomy

The differences between the anatomical structures in the four models were compared based on visual appearance, including size, shape, and color. Macroscopic photos were acquired.

Histology

In human *post mortem* and swine, nerve tissue was resected and surgical biopsies from the surrounding tissues were acquired for histological analysis. The histological slides were stained using standard hematoxylin and eosin.

Instrumentation

Fiber optic probes, including one illumination fiber and one collecting fiber (Invivo Germany, Schwerin, Germany) were used to deliver broad spectrum light from a tungsten-halogen source. The diffusely reflected light, measured *via* the collecting fiber, was analyzed in the range of 400–1,600 nm by two spectrometers (DU420A-BRDD and DU492A-1.7, Andor Technology, Belfast, Northern Ireland) covering the visible and near-infrared range. The distance between the illumination and collection fiber was 0.8 mm, the probe diameter at the tip was 2.0 mm. The setup is schematically represented in Figure 1. The measurement setup is controlled by a custom made LabView software interface (National Instruments, Austin, TX). The instrumentation and calibration procedure of the DRS system has been described in detail elsewhere [13].

Spectral Analysis

A widely accepted analytical model, first described by Farrell et al., was used to quantify validated physiological, morphological, and metabolic parameters within the measured tissue [14]. These parameters include volume fractions or concentrations of the different chromophores and scattering parameters. The implementation of this model to analyze diffuse reflectance spectra over a wavelength of 400–1,600 nm is described by Nachabé [13]. The analytical model was implemented into a Matlab software environment (Matworks Inc., Natrick, MA).

Spectra used to fit the measured profile were from oxy- and deoxyhemoglobin, fat, water, β -carotene, and collagen. Further, the effects of both Mie- and Rayleigh scattering, the scattering slope (b) and α on the spectrum were estimated. In the analysis, outliers were defined as greater

than $q_3 + (q_3 - q_1)$ or smaller than $q_1 - (q_3 - q_1)$ with q_1 the 25th and q_3 the 75th percentile.

Classification

To evaluate whether classification algorithms intended for human *in vivo* can be trained and optimized on alternative models, we trained a 3-knn classification on each of the three alternative models and classified the human *in vivo* data with this algorithm. The classification results in terms of sensitivity, specificity and Matthews correlation coefficient (MCC) were compared with the classification of the human *in vivo* measurements using a cross-validation scheme. The MCC is used in machine learning as a measure of quality of classifications [15]. Per model, two classification runs were performed: one with all fitted parameters, the second with a subset of parameters. The parameter subset consists of the most distinctive parameters in the *in vivo* human cross-validation. The parameters in the subset were selected based on the effect on the classification result (MCC) after systematic omission of individual parameters.

RESULTS

Anatomy

Macroscopically, the difference between human and swine is most notable in size; the diameter of the investigated nerves in human was approximately twice the diameter of the swine nerves. In comparison to swine, the appearance of human nerve shows small ribs, or grooves (Fig. 2), which may vary per case. There were no significant differences in appearance between human *in vivo* and *post mortem* specimens or swine *in vivo* and *post mortem* samples.

In the surrounding tissue, the amount of blood differs between the models. By eye, the most blood can be found in living human, followed by *in vivo* swine, human *post mortem*, and swine *post mortem*. The color of the subcutaneous fat differed between the specimens. The subcutaneous fat in human cadaver was yellow, in swine (both *in vivo* or *post mortem*) was almost white, and human *in vivo* was yellow-white.

Histology

In histology, both human and swine nerves were composed of fascicles, enclosed by perineurium. A nerve (branch) is surrounded by an outer layer of connective tissue, the outer epineurium, which is surrounded by a fatty layer: sliding fat. Within the outer epineurium, fascicles are accompanied by adipocytes and loose connective tissue (inner epineurium). Within the inner epineurium, no differences were found in cell type or density between human or swine nervous tissue. While nerve and fat tissue (adipose tissue) showed clear similarities between human and swine, differences at the histological level were found in muscle. The density of muscle fibers in swine was remarkably higher compared to human. In human muscle considerably more adipocytes and endomyxial collagen surrounded the muscle fibers. Histological

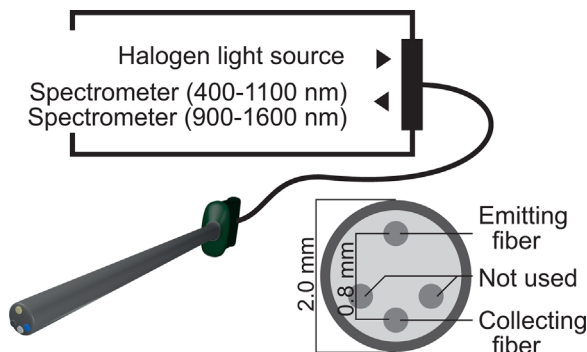


Fig. 1. Schematic of the measurement setup and probe. The tip of the probe is visualized at the right.

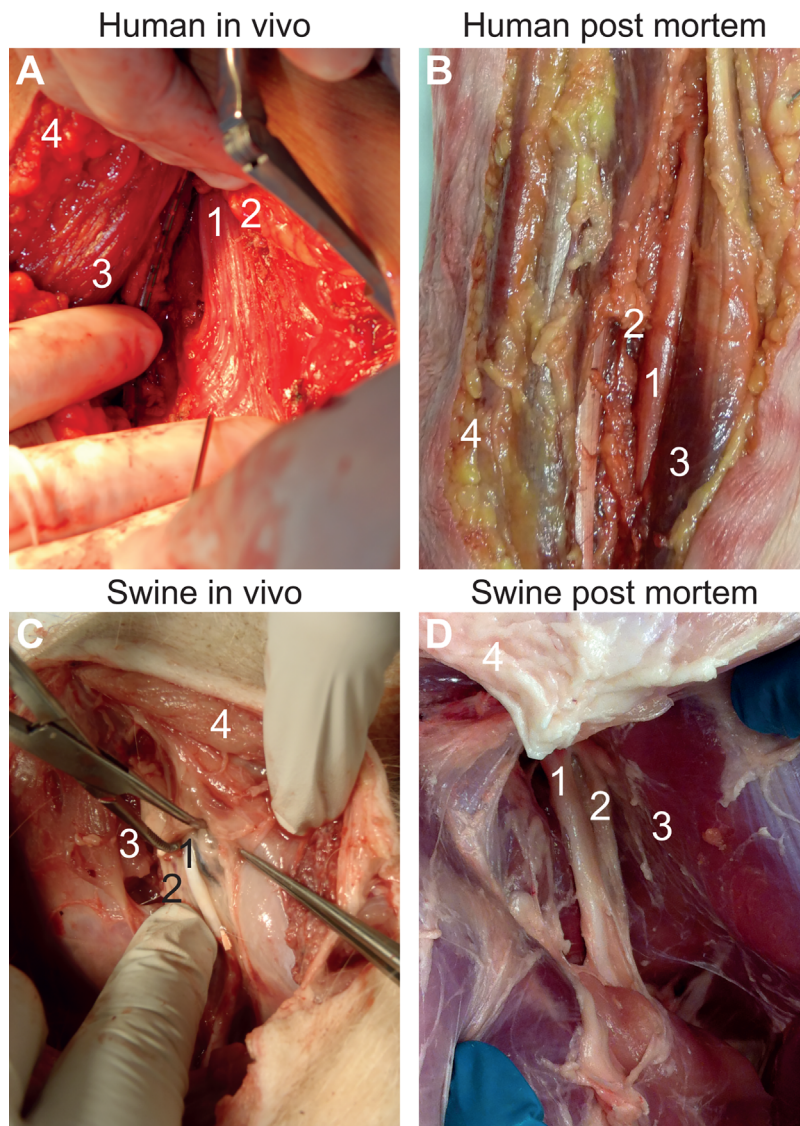


Fig. 2. Macroscopic images of the four models (A human *in vivo*, B human post mortem, C Swine *in vivo*, D Swine post mortem). All images show the sciatic nerve and surrounding tissue: 1. Sciatic nerve, 2. Slide fat, 3. Muscle, 4. Subcutaneous fat.

images of nerve and surrounding tissue for human and swine are displayed in Figure 3.

Optical Parameters

Optical spectra. Typical examples of the measured spectra were visualized in Figure 4. Interpretation of DRS spectra, and an analysis of the spectra characteristics is discussed elsewhere [5].

General trends. The measured values of the optical parameters are visualized in Figure 5; measurements are grouped per tissue type and model. The significance of the differences in parameter values, based on a Kruskal Wallis test, are shown in Table 1.

When comparing nerve with surrounding tissue, the optically measured parameters show comparable trends

throughout the four models. On nerve measurements show intermediate amounts of fat, that are high compared with muscle, but low when compared with sliding fat or subcutaneous fat. With regard to the amount of blood, which can only be judged reliably during *in vivo* measurement, on nerve measurements show higher amounts of blood compared to adipose tissues (sliding fat and subcutaneous fat) but low compared to muscle. Muscle shows high levels of blood and water, with the lowest level of oxygen saturation in all four models. The adipose tissues (subcutaneous fat and sliding fat) are characterized by a high amount of fat and relatively low amounts of water and blood. β -carotene is absent in all swine measurements.

Human in vivo versus post mortem. The human *post mortem* measurements contain generally more blood

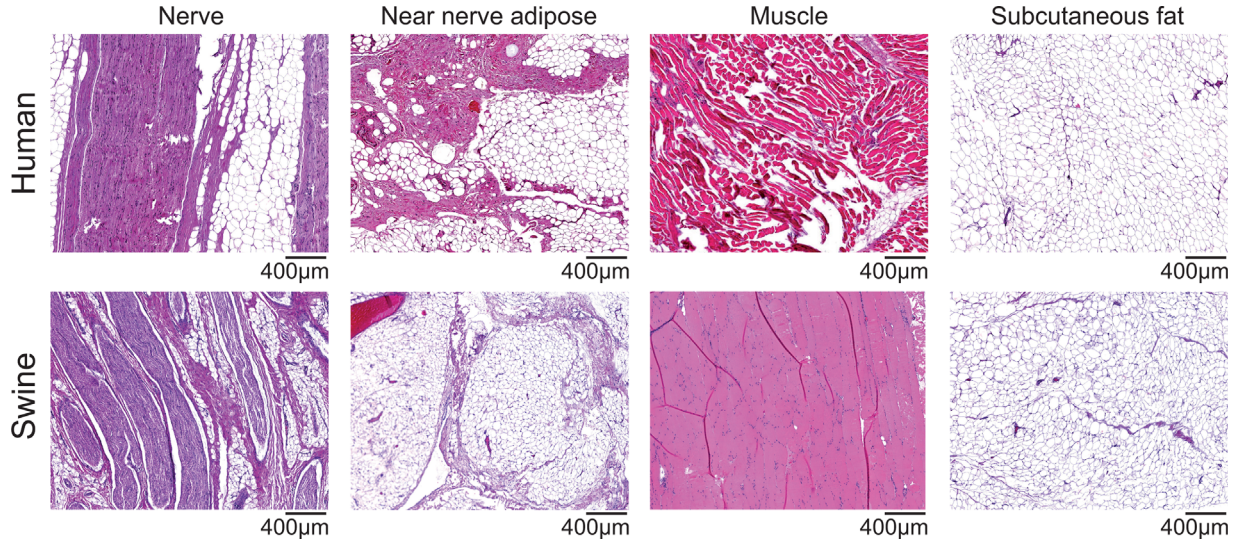


Fig. 3. Histological samples for the investigated tissue in both human and swine. The upper row holds images from human tissue, the lower row from swine. Columns represent nerve, near nerve adipose tissue, muscle, and subcutaneous fat.

compared with the other models, whereas the variation in oxygen saturation is less pronounced in human *post mortem*. For on nerve measurements, the content of water and fat appear slightly lower for *post mortem* compared to *in vivo*.

Human in vivo versus swine in vivo. For on nerve measurements, the fat fraction measured lower in swine compared to human. Slightly less blood was measured in swine and also the sum of the water and fat volume fraction was lower compared to human. In contrast, for muscle the sum of the water and fat volume fraction was higher for swine compared to human. As for nerve tissue, the amount of blood and the oxygen saturation in muscle were lower in

swine compared to human. In adipose tissue *in vivo* measurements of water, fat, and blood content were not different for human or swine.

Human in vivo versus swine post mortem. The on nerve measurements showed great similarities between human *in vivo* and swine *post mortem* for the amounts of water and blood. The fat content in swine nervous tissue measured lower compared to human. Both subcutaneous fat and sliding fat showed water content comparable to their human *in vivo* equivalent. For muscle, human *in vivo* contained more blood compared to swine *post mortem*.

Classification

The classification results for training on an alternative model and validation in human *in vivo* are summarized in Table 2. Cross validation within the human *in vivo* group resulted in an MCC of 0.6 with a sensitivity of 81% and a specificity of 80%. The most distinctive parameters were oxygen saturation, the amount of water and fat and the ratio between them, concentrations of hemoglobin and the amount of Mie scattering.

Training the classification algorithm on another model combined with classification on *in vivo* human indicates the similarity between the two models. In case of maximum resemblance, the accuracy will be comparable to cross-validation within *in vivo* human. All classifications resulted in an MCC well above 0, indicating a positive correlation. Training was performed using all available parameters but also using only a subset of parameters that were most distinctive in the human cross-validation. The limitation for the classification to use only the parameter subset from the *in vivo* human cross validation did not result in substantially lower scores. The classification of nerve tissue for human *ex vivo* and swine *in vivo/ex vivo* showed minimal differences in MCC and accuracy.

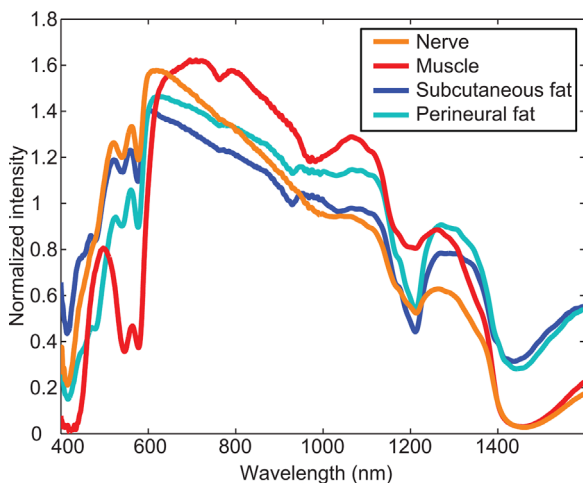


Fig. 4. Typical examples of DRS spectra measured on nerve, muscle, subcutaneous fat, and perineural fat. The spectra were acquired in human *post mortem*.

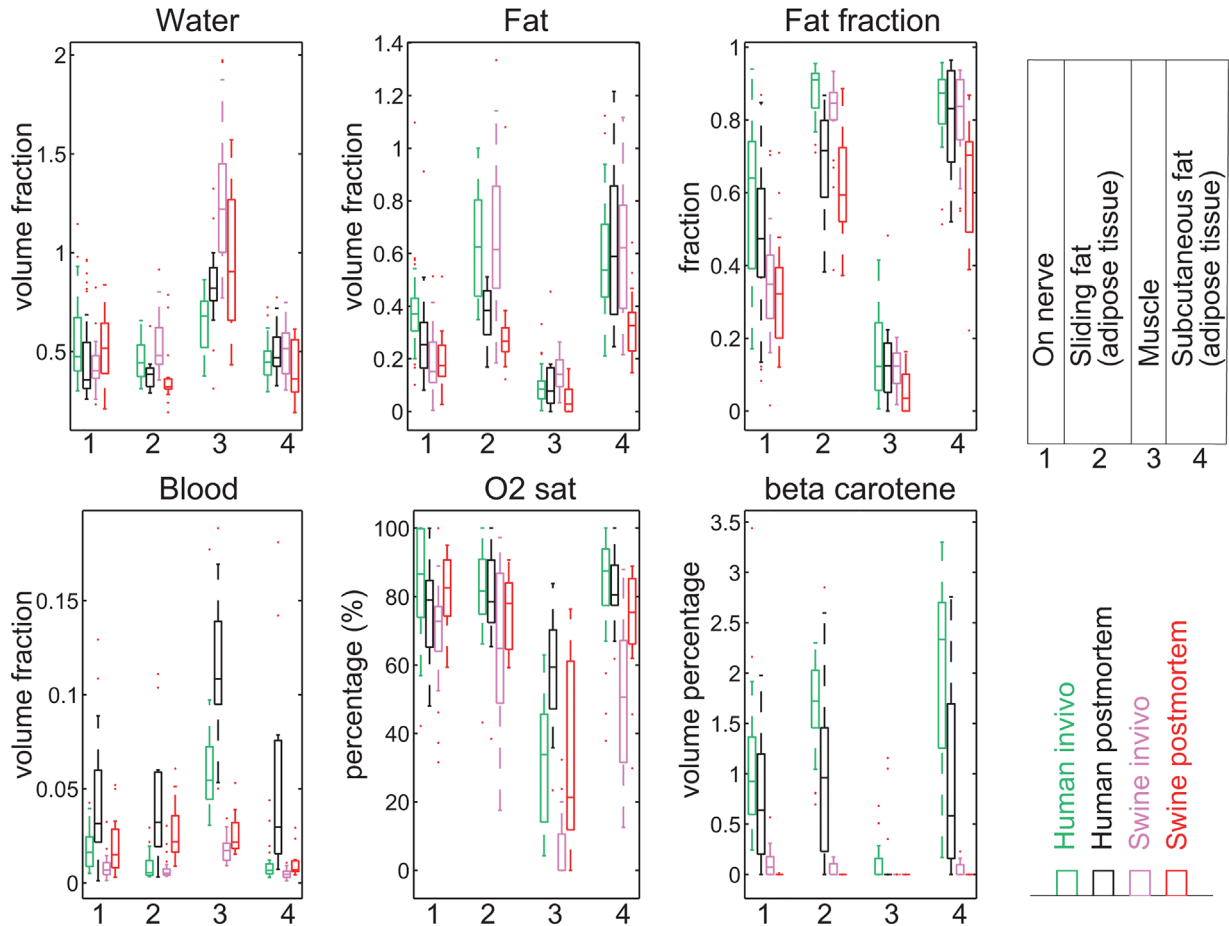


Fig. 5. Parameters based on optical measurements, visualized as boxplots. Hemoglobin oxygen saturation is denominated as O₂ sat. The horizontal line in the box represents the median values; the box marks the 25th and 75th percentiles. Outliers are marked with red dots.

DISCUSSION

Optical nerve identification techniques like DRS aim to fulfill a clinical demand on tissue identification at the tip of an instrument. Due to the small size of optical fibers, the technique could be integrated into surgical tools. During surgery, DRS may help to prevent nerve damage using surgical tools with optical tissue identification at the tip of the instrument. Multiple surgical instruments establish solid tissue contact prior to dissection and are therefore eminently suited for tissue identification. Examples are surgical staplers, harmonic scalpels [16], and vessel sealing devices [17]. In other medical areas, instruments with integrated optical fibers were also subject of research, an example is a tool for tissue biopsy used in radiology [18]. In regional anesthesia, feedback on the tissue type at the tip of a needle may improve accurate deposition of the analgesic around the nerve and therefore improve the quality and onset of a regional nerve block. A prototype of a needle stylet with integrated optical fibers was used presented earlier. The potential of optical techniques to identify nervous tissue was demonstrated by several

authors [3–8,19]. Nerve tissue was discriminated between several surrounding tissue including bone and glandular tissue [7], muscle and adipose tissue [5,6,8], and blood vessel [19]. All these studies show good classification results, but none of them reaches perfect (100%) tissue identification. Furthermore, these studies were performed in a controlled setting.

To move the technique from a controlled experimental setting into a mature clinically applied device is a long process that will require multiple optimization and validation cycles. Not all these cycles are necessarily executed in humans *in vivo*. In recent literature several models have been described including human *post mortem* [5], and swine *in vivo* [3]. Ideally, the optical properties and measured parameters in such models should closely resemble their human *in vivo* equivalent. A systematic comparison of optical properties between the different models would be useful for a broad range of optical techniques. This study aims to expose and understand the similarities and differences to validate nerve measurements between human *in vivo*, human post mortem, swine *in vivo*, and swine *post mortem*. Nerve and surrounding

TABLE 1. Optically Measured Concentration

Parameter	<i>In vivo</i> human (mean)	<i>Ex vivo</i> human	<i>In vivo</i> swine	<i>Ex vivo</i> swine
Nerve				
Water (vol. frac)	0.55	≈	≈	=
Fat (vol. frac)	0.39	↓	↓	↓
Fat/(water + fat)	0.57	=	↓	↓
Hemoglobin (mg/ml)	2.67	↑	↓	=
O ₂ sat (%)	84.99	≈	≈	=
β-carotene (×10 ⁻⁸ Mol)	1.01	=	↓	↓
Sliding fat				
Water (vol. frac)	0.46	=	=	≈
Fat (vol. frac)	0.63	↓	=	↓
Fat/(water + fat)	0.88	↓	=	↓
Hemoglobin (mg/ml)	1.29	↓	=	↑
O ₂ sat (%)	81.30	=	=	=
β-carotene (×10 ⁻⁸ Mol)	1.65	=	↓	↓
Muscle				
Water (vol. frac)	0.65	≈	↑	≈
Fat (vol. frac)	0.10	=	≈	≈
Fat/(water + fat)	0.15	=	=	≈
Hemoglobin (mg/ml)	9.36	↑	↓	↓
O ₂ sat (%)	31.85	↑	↓	=
β-carotene (×10 ⁻⁸ Mol)	0.12	=	=	=
Subcutaneous fat				
Water (vol. frac)	0.45	=	=	=
Fat (vol. frac)	0.59	=	=	↓
Fat/(water + fat)	0.83	=	=	↓
Hemoglobin (mg/ml)	1.50	↑	≈	=
O ₂ sat (%)	82.74	=	↓	=
β-carotene (×10 ⁻⁸ Mol)	2.05	≈	↓	↓

Significant differences (Kruskal Wallis P -value < 0.001) are indicated by ↑ or ↓. P -values of > 0.01 indicate that the groups show great similarity (=). P -values > 0.001 and < 0.01 are considered not significantly different (≈). vol. frac, volume fraction. O₂ sat, Hemoglobin oxygen saturation.

tissue were compared between human and swine macroscopically, histologically, and in optical parameters measured by DRS. This could be of value when choosing a model to validate optical techniques for nerve identification.

Macroscopic examination of the tissue revealed differences in the color of adipose tissue between human and swine. The yellow color of adipose tissue is related to the β-carotene concentration [20]. In general, mammals are categorized as either white-fat or yellow-fat animals: the

TABLE 2. The 3-knn Classification Was Trained on the Data of Human *Ex Vivo*, and Swine *In-* and *Ex Vivo* and Validated on the Human *In Vivo* Dataset as a Measure for the Similarities Between the Models

Model	MCC	Sensitivity (%)	Specificity (%)	Accuracy
Human <i>in vivo</i> (cross validation)	0.60	81	80	0.80
Human <i>ex vivo</i>				
All parameters	0.47	61	84	0.73
Parameter subset	0.44	73	71	0.72
Swine <i>in vivo</i>				
All parameters	0.46	39	98	0.69
Parameter subset	0.41	42	93	0.68
Swine <i>ex vivo</i>				
All parameters	0.46	63	82	0.73
Parameter subset	0.43	51	89	0.71

All available fit-parameters as well as the subset of parameters selected in the *in vivo* human cross validation were used as inputs to the models.

carotenoid content and color of adipose tissue in yellow-fat animals is due to their ability to absorb, transport and store carotenoids, whereas white-fat animals lack this ability; humans have yellow fat, while pigs, rats, and mice have white-fat [21].

The quantified amount of blood in the tissue shows model dependency. The amount of blood is consistently high in human *post mortem* and low for swine *in vivo*. The low amount in swine *in vivo* might be due to the low arterial blood pressure during surgery; advised mean arterial pressure (MAP) in swine is 60–70 mmHg [22]. Compared to surgery in humans, smaller decrease of arterial pressure is allowed. A decrease of systolic arterial pressure (SAP) higher than 20% is often chosen to define perioperative hypotension in human [23]. Post mortem, the coagulation is disturbed for several reasons including temperature. In swine post mortem, the blood is drained, in human *post mortem* the body still contains substantial amounts of blood. *Post mortem* the distribution of blood between veins and arteries is shifted toward the venous system, also increasing the blood volume in capillaries [24]. As the coagulation system is largely disturbed post mortem, increased bleeding during preparation occurs. The combination of these factors may lead to the high measurements for the blood parameter in human *post mortem* compared to *in vivo* and low in swine *post mortem*.

Related to the amount of blood is the hemoglobin oxygen saturation. In *post mortem* tissue, cellular metabolism is assumed to have ceased, and oxygen is no longer consumed. Meanwhile, tissue preparation provides exposure to room air allowing the hemoglobin to saturate with oxygen, analogous to the increase in oxygen saturation if an air bubble is trapped in a blood gas syringe [25]. However, the measured oxygen saturation still shows low oxygen saturation in muscle. Although the difference in oxygen saturation between nerve and muscle is lower in the *post mortem* measurements, muscle tissue still shows lower values. A possible explanation is the presence of methemoglobin within the *post mortem* muscle; methemoglobin is the oxidized form of hemoglobin and could increase *post mortem* [26]. The presence of methemoglobin may influence the estimation of the oxygen saturation. Currently, methemoglobin is not included in the fitting algorithm.

The typical age of the specimen in the four different models (human *in/ex vivo*, swine *in/ex vivo*) differs. Human cadavers available for research are typically older than patients undergoing surgery. Swine used for training surgical procedures are typically full grown where domestic slaughter pigs are typically 3–8 months old. The differences in age may have had an impact on the histological appearance of the muscle tissue; the amount of adipocytes and endomysial collagen in human muscle was clearly higher compared to swine. Intramuscular connective tissue, including perimysium and endomysium, is known to increase with age [27]. In this research, patients and specimens were not selected based on age. Patients and specimens represent the typical age in their group.

CONCLUSION

In this study, three alternative models for the development of optical techniques for nerve identification were examined. Differences in macroscopy, histology and optically derived parameters were compared between human *in vivo* and the alternative models. Despite differences in appearance and histology, similarity between optical parameters is sufficient to yield a strong positive correlation after cross model classification. The presented similarities and differences could be of value in optical tissue recognition techniques like DRS, multispectral camera's and Raman spectroscopy, especially when choosing a model for validation and optimization. When the distinguishing features of an identification algorithm are known, an alternative model could be selected with maximum similarities to human *in vivo* regarding these features.

ACKNOWLEDGMENTS

The authors would like to thank Lisanne de Boer, Rachele Snellen, Danielle op den Kamp, Dr. Imo E. Hoefler, and the Animal facility of the Utrecht University for assistance during the measurements. For this study, the Netherlands Cancer Institute received an unrestricted grant from Philips Research. This research was further supported by a grant of the KWF-Alpe d'HuZes (NKI 2014-6596). The Maastricht University Medical Center received unrestricted research funding from Philips to carry out the work. The author affiliated with this institution (A.B.) received no payment for participation in this research project.

REFERENCES

1. Urmev WF, Stanton J. Inability to consistently elicit a motor response following sensory paresthesia during interscalene block administration. *Anesthesiology* 2002;96(3):552–554.
2. Perlas A, Niazi A, McCartney C, Chan V, Xu D, Abbas S. The sensitivity of motor response to nerve stimulation and paresthesia for nerve localization as evaluated by ultrasound. *Region Anesth Pain M* 2006;31(5):445–450.
3. Brynolf M, Sommer M, Desjardins AE, et al. Optical detection of the brachial plexus for peripheral nerve blocks: An *in vivo* swine study. *Region Anesth Pain M* 2011;36(4):350–357.
4. Desjardins AE, Van der Voort M, Roggeveen S, et al. Needle stylet with integrated optical fibers for spectroscopic contrast during peripheral nerve blocks. *J Biomed Opt* 2011;16(7):077004.
5. Hendriks BH, Balthasar AJ, Lucassen GW, et al. Nerve detection with optical spectroscopy for regional anesthesia procedures. *J Trans Med* 2015;13(1):380.
6. Schols RM, ter Laan M, Stassen LP, et al. Differentiation between nerve and adipose tissue using wide-band (350–1,830 nm) *in vivo* diffuse reflectance spectroscopy. *Laser Surg Med* 2014;46(7):538–545.
7. Stelzle F, Knipfer C, Bergauer B, et al. Optical nerve identification in head and neck surgery after Er: YAG laser ablation. *Laser Med Sci* 2014;29(5):1641–1648.
8. Balthasar A, Desjardins AE, van der Voort M, et al. Optical detection of peripheral nerves: An *in vivo* human study. *Region Anesth Pain M* 2012;37(3):277–282.
9. Schols RM, Dunias P, Wieringa FP, Stassen LP. Multispectral characterization of tissues encountered during laparoscopic colorectal surgery. *Med Eng Phys* 2013;35(7):1044–1050.
10. Langhout GC, Spliethoff JW, Schmitz SJ, et al. Differentiation of healthy and malignant tissue in colon cancer patients

- using optical spectroscopy: A tool for image-guided surgery. *Laser Surg Med* 2015;47(7):559–565.
11. Evers DJ, Nachabe R, Peeters M-JV, et al. Diffuse reflectance spectroscopy: Towards clinical application in breast cancer. *Breast Cancer Res Tr* 2013;137(1):155–165.
 12. Langhout GC, Kuhlmann KFD, Wouters MWJM, et al. Nerve detection during surgery: Optical spectroscopy for peripheral nerve localization. *Laser Med Sci* 2017; in press.
 13. Nachabé R, Evers DJ, Hendriks BH, et al. Diagnosis of breast cancer using diffuse optical spectroscopy from 500 to 1600 nm: Comparison of classification methods. *J Biom Opt* 2011;16(8):8087010–8087012.
 14. Farrell TJ, Patterson MS, Wilson B. A diffusion theory model of spatially resolved, steady-state diffuse reflectance for the noninvasive determination of tissue optical properties in vivo. *Med Phys* 1992;19(4):879–888.
 15. Powers DM. Evaluation: From precision, recall and F-measure to ROC, informedness, markedness and correlation. *J Mach Learn Tech* 2011;2(1):37–63.
 16. Miccoli P, Berti P, Dionigi GL, D'Agostino J, Orlandini C, Donatini G. Randomized controlled trial of harmonic scalpel use during thyroidectomy. *Arch Otolaryngol Head Neck Surg* 2006;132(10):1069–1073.
 17. Landman J, Kerbl K, Rehman J, et al. Evaluation of a vessel sealing system, bipolar electrosurgery, harmonic scalpel, titanium clips, endoscopic gastrointestinal anastomosis vascular staples and sutures for arterial and venous ligation in a porcine model. *J Urology* 2003;169(2):697–700.
 18. Spliethoff JW, Prevoo W, Meier MA, et al. Real-time *in vivo* tissue characterization with diffuse reflectance spectroscopy during transthoracic lung biopsy: A clinical feasibility study. *Clin Cancer Res* 2016;22(2):357–365.
 19. Balthasar A, Desjardins AE, van der Voort M, et al. Optical detection of vascular penetration during nerve blocks: An *in vivo* human study. *Region Anesth Pain M* 2012;37(1):3–7.
 20. Wu L, Guo X, Wang W, et al. Molecular aspects of β , β -carotene-9', 10'-oxygenase 2 in carotenoid metabolism and diseases. *Exp Biol Med* 2016;241(17):1879–1887.
 21. Krinsky NI, Mayne ST, Sies H. In: Carotenoids in health and disease. New York, United States: Taylor & Francis Inc (CRC press); 2004. p 576.
 22. Swindle MM, Smith AC. In: Swine in the laboratory: Surgery, anesthesia, imaging, and experimental techniques. New York, United States: Taylor & Francis Inc (CRC press); 2015.
 23. Lonjaret L, Lairez O, Minville V, Geeraerts T. Optimal perioperative management of arterial blood pressure. *Integr Blood Press Control* 2014;7:49.
 24. Koeppen B, Stanton BA. In: Berne and levy physiology. Atlanta, United States: Elsevier Inc; 2008. p 394.
 25. Biswas C, Ramos J, Agroyannis B, Kerr D. Blood gas analysis: Effect of air bubbles in syringe and delay in estimation. *Br Med J* 1982;284(6320):923–927.
 26. Reay DT, Insalaco SJ, Eisele J. Postmortem methemoglobin concentrations and their significance. *J Forensic Sci* 1984;29(4):1160–1163.
 27. Fang S, Nishimura T, Nishimura T. Relationship between development of intramuscular connective tissue and toughness of pork during growth of pigs. *J Anim Sci* 1999;77(1):120–130.